Simulating interactions between topography, permafrost, and vegetation in Siberian larch forest

Environmental Research Letters

PAPER

Simulating interactions between topography, permafrost, and vegetation in Siberian larch forest

Hisashi Sato(佐 藤 永)[1,5], **Hideki Kobayashi**(小林 秀樹)[1], **Christian Beer**[2] **and Alexander Fedorov**[3,4]

[1] Japan Agency for Marine-Earth Science and Technology (JAMSTEC), Yokohama, JAPAN
[2] Stockholm University, Stockholm, Sweden
[3] Melnikov Permafrost Institute, Yakutsk, Russia
[4] North-Eastern Federal University, Yakutsk, Russia
[5] Author to whom any correspondence should be addressed.

E-mail: hsatoscb@gmail.com

Keywords: Permafrost, Siberian larch, TOPMODEL

Supplementary material for this article is available online

OPEN ACCESS

RECEIVED
9 March 2020

REVISED
3 June 2020

ACCEPTED FOR PUBLICATION
11 June 2020

PUBLISHED
2 September 2020

Abstract

In eastern Siberia, topography controls the abundance of the larch forest via both drought and flooding stresses. For the reconstruction of these topographical effects, we modified a dynamic vegetation model to represent soil water relocation owing to within-grid heterogeneity of elevation, over-wet-kill of trees, and air temperature differences within-grid. After calibration, the model reasonably reconstructed the geographical distributions of observation-based-estimates of fundamental properties of plant productivity and thermo-hydrology. Thus, the model appropriately responded to environmental gradients in eastern Siberia. The modified model also partially reconstructed the topography control on tree abundance and thermo-hydrology status in eastern Siberia, although its geographical distribution was not always good. In the modified model, soil water redistribution increased the risk of over-wet-kill in lower elevation classes, whereas it reduced the risk of over-wet-kill for larch trees in higher elevation classes. We demonstrated that without considering the latter effect, forest collapse due to over-wet stress would happen throughout eastern Siberia under a forecasted climatic condition during the 21st century, which will deliver a much moister environment throughout eastern Siberia. Therefore, modeling the over-wet-kill of trees without considering topographical heterogeneity would result in the overestimation of forest collapse caused by the over-wet-kill of trees under an expected climate trend in eastern Siberia.

1. Introduction

In eastern Siberia, larches (Larix spp.) often exist in pure stands, constructing the world's largest coniferous forest (Schulze *et al* 1995), to which changes can significantly affect the earth's albedo and global carbon balance (Bonan *et al* 1995, Gibbard *et al* 2005). Siberian larch forest is located in an extreme environment for the existence of a forest ecosystem; hence, small differences in environmental conditions will alter its presence. There is a quantitative pattern that topographic properties control the abundance of larch forest via both drought and flooding stresses in this region; larch abundance appears to be constrained by drought stress in mountainous regions, but flooding stresses in plain areas (Sato and Kobayashi 2018).

The larch-dominated region in Siberia is underlaid by permafrost and plant productivity is partially under the control of active layer thickness (ALT); deeper ALT increases the water holding capacity of soil, thereby enhancing plant productivity (Beer *et al* 2007, Sato *et al* 2016, but see also Zhang *et al* 2011). Soil wetness inversely influences ALT. For example, the greater ice content in the soil of moister areas facilitates upward heat conduction from the permafrost, which results in a shallower ALT (Woo and Xia 1996, Carey and Woo 1998). Such a thermo-hydrological system is expected to change drastically because the arctic region has warmed more than twice as fast as the global average (Cohen *et al* 2014) and near-surface permafrost and seasonally frozen ground areas are projected to decline substantially during the 21st century (Lawrence and Slater 2005).

Therefore, for the quantitative reconstruction and projection of geographical distribution and functions of the Siberian larch forest, topography and thermo-hydrological dynamics mediated heterogeneity of the environment should be taken into consideration. Previous studies have focused on modeling the influences of thermo-hydrological dynamics on larch forest using process-based models (Beer *et al* 2007, Zhang *et al* 2011, Sato *et al* 2016). However, topography mediated heterogeneities of the environment within simulation grids were often neglected.

Kleinen *et al* (2012) integrated a dynamic vegetation model, LPJ-DGVM with a wetland module, which dynamically determines the fraction of inundated areas and probability density function (PDF) of the water-table-depth within each simulation grid. Then, this integrated model simulates peat accumulation, which can only happen in water-saturated areas. This wetland module is based on TOPMODEL, which is a physically based streamflow and water-table-depth computational scheme. TOPMODEL calculates hydrological heterogeneity within watersheds; it inputs water-table-depth averaged over the watershed and a PDF of the combined topographic index (CTI) and then outputs the mean watershed base flow and a PDF of water-table-depth (Beven and Kirkby 1979, Stieglitz *et al* 1997, Gedney and Cox 2003).

In this study, a dynamic vegetation model, SEIB-DGVM (Sato *et al* 2016), which works with a thermo-hydrology land-physics-model NOAH-LSM 2.7.1 (Ek *et al* 2003), was extended for the reconstruction of the topography-mediated-heterogeneity of this environment within simulation grid cells. This extension was achieved by the implementation of the TOPMODEL. After the calibration of the model for eastern Siberia, we conducted a model experiment to quantitatively understand how plants, thermo-hydrology, and topography work together. Then, we adapted the model to a forecasted climatic condition at the end of the 21st century and evaluated how these modifications alter the prediction of the abundance of the Siberian larch forest.

Specifically, we addressed the following questions. (1) Do the model modifications contribute to the reconstruction of topography control on thermo-hydrology and tree abundance in eastern Siberia? (2) Is the mechanism that is responsible for the reconstruction consistent with observation trend? (3) How do the model modifications change the projection of tree abundance in eastern Siberia at the end of the 21st century?

2. Method

2.1. The original model

All simulations in this study were conducted by the integrated model of the SEIB-DGVM (Sato *et al* 2016), which reconstructs plant and carbon dynamics under specified climatic conditions, and the one-dimensional (i.e. not considering the lateral flow of water and heat) land-surface-model NOAH-LSM to mechanistically link thermo-hydrology with plant dynamics. In the model, vegetation fraction controls incoming solar radiation and surface heat flux conductance on top of the soil layer. Soil moisture and its state (liquid or solid) influence both hydraulic conductance and heat conductance, and thereby feedback to soil moisture and its state. This integrated model roughly reconstructs the latitudinal gradients for permafrost presence, soil moisture, canopy leaf area index (LAI), and biomass over the entire larch-dominated area in eastern Siberia.

Sato *et al* (2016) provides a full description of this integration. Here, we only outline the integrated-model and describe the modifications made for this study. The simulation unit of the model is spatially explicit; a 30 m $\times$ 30 m 'virtual forest' in which individual trees establish, compete, and die. The ground is vertically divided into 20 soil layers, each 0.1 m deep. Plant dynamics in the virtual forest work in conjunction with the carbon and water cycles. In the integrated model, the SEIB-DGVM provides the NOAH-LSM with daily updates of LAI and vegetation fraction, whereas the NOAH-LSM provides the SEIB-DGVM with daily updates of the vertical profiles of soil wetness and temperature.

The Siberian larch forest generally suffers from severe nitrogen deficiency (Schulze *et al* 1995), which limits leaf carbon gain (Vygodskaya *et al* 1997). However, the model does not consider nitrogen limitation on plant growth; hence, our model might overestimate the CO_2 fertilization effect.

2.2. Model modifications

The simulation area is in the Sakha Republic of Russia, which corresponds to the geographical extent to which permafrost temperature and ALT data (Beer *et al* 2013) are available. Each simulation grid, at the resolution of 0.5-degree, was divided into 56 $\times$ 56 pixels (1/112-degree resolution), which corresponds to calibration and validation datasets. Land pixels of each simulation grid were sorted in ascending order of elevation and almost equally divided into 10 groups (hereafter, referred to as 'elevation rank'). Elevation rank of each simulation grid is represented by a single model simulation, assuming that all pixels at the same elevation ranked in a simulation grid share identical environmental conditions. As all elevation ranks represent nearly the same number of pixels, we regard stated variables averaged over the elevation rank as grid representing values.

Therefore, within-grid heterogeneity was only controlled by elevation in the modified model. This assumption was rationalized by (1) considering that elevation is the most straightforward way to implement within-grid heterogeneity of air temperature and (2) elevation tightly correlates with slope and soil

depth profiles, all of which control hydrology, and tightly correlates with the flooding record in eastern Siberia (Sato and Kobayashi 2018).

TOPMODEL, which dynamically determines the heterogeneity of water-table-depth within a watershed, was employed in this study. Instead of detailed topographic properties, TOPMODEL requires a CTI, which is defined to be ln (α_i/tan (β_i)), where α_i is area draining through location i per unit contour length, and β_i is the local slope at that location. α_i and tan(β_i) can be regarded as, respectively, a dimensionless index for the area draining through location i, and a measure of how fast water can be transported downslope through that location. Regarding a simulation grid as a watershed, we calculated the mean CTI value using Marthews *et al* (2015) for each elevation rank of each simulation grid. As there are negative correlations between CTI and elevation throughout the simulation area (mean $r^2 = -0.286$, $n = 2678$), the elevation rank partially reflects the difference in CTI within each grid.

The specific procedure for the implementation of TOPMODEL into the SEIB-DGVM is explained in the supplemental information (SI) 1 (available online at stacks.iop.org/ERL/15/095006/mmedia). With the redistribution of soil water among elevation ranks, the air temperature of each elevation rank is adjusted by subtracting 0.6 °C for every 100 m higher elevation than the grid average. The bottom soil temperature at a depth of 2 m was taken from the observation of permafrost temperature by Beer *et al* (2013) and was assumed to be constant. This assumption is only due to technical reason for reducing computation demands. We should note that it will result in the underestimation of the rate at which permafrost thaws under a warming trend, and it ignores possibility of rapid landscape changes (e.g. thermokarsting and plateau subsidence) those can happen as a result of permafrost decay (Walvoord and Kurylyk 2016).

In the original model, trees can die due to the low-growth-efficiency (carbon starvation) and bioclimatic-limits. We additionally introduced death by over-wet stress; 20% of individual trees die when the monthly mean soil water within 50 cm of the active layer exceeds 74% of its soil-saturation-point. This evaluation of over-wet stress is conducted at the end of each month during the leafing period of larch. This formulation is a result of model calibration based on the observational data. Detail procedures are described in SI2.

2.3. Data

The model requires daily climatic variables for the following items: mean air temperature, daily range of air temperature, precipitation, downward shortwave and longwave radiations, wind velocity, and relative humidity. For the calibration and validation of the model, we employed historical climate data from the period between 1991 and 2000, which was mainly delivered from CRU-TS4.00 observation-based climatic data (0.5 Degree, 1901 ∼ 2015) (Harris *et al* 2020). During this period, number of meteorological station contributed to the CRU data is relatively stable in Russia (Harris *et al* 2014), and this period overlaps ranges those major validation datasets cover (larch LAI: 1998–2013, GPP: 1998–2005). As CRU data are provided at monthly time intervals, daily climatic variability within each month was supplemented using NCEP/NCAR daily climate data (Kalnay *et al* 1996). For daily wind data, NCEP/NCAR reanalysis was employed for simulations. For radiations, we made corrections based on the NASA/GEWEX SRB Release-3.0 monthly dataset (https://eosweb.larc.nasa.gov/project/srb/srb_table). SI3 explains the specific and detailed procedure of data conversion.

In the simulations for the 21st century projection, we used an MIROC-AOGCM output under the RCP8.5 scenario (Watanabe *et al* 2011). The spatial resolution of this AGCM output was 192 × 94 global grids and was linearly interpolated to a 0.5° grid mesh, which corresponds to the spatial resolution for the simulations in this study. To provide consistency for the historical climate data, the 21st century data of MIROC were converted using the 20th century data of CRU; for each climatic item by month, averages from 1991 to 2000 data were subtracted from the 21st century projections of the MIROC and the averages from 1991 to 2000 of the CRU were added. Because the AGCM data are also provided as monthly time interval, daily climatic variability within each month was supplemented in the same way as the historical climate data. Geographical distributions of annual precipitation and annual mean air temperature of historical and future conditions are shown in figure S1.

The model requires elevation, CTI, and permafrost temperature as forcing data (figure 1, table S1). For the calibration and validation of the model, we employed tree LAI, gross primary production (GPP), living biomass, active layer thickness (ALT), and runoff fractions (figure 2, table S2). Elevation, CTI, permafrost temperature, and ALT were converted to 1/112° using the assumption that these environmental variables are linearly changed between proximate grids. This resolution corresponds to the Larch-LAI data, which have the coarsest resolution among these datasets.

2.4. Calibration and validation

For the calibration and validation of the model, we used a simulated forest of 100 years, which can be regarded as the average forest age of a Siberian larch forest, because the average interval of stand-replacing fire of a Siberian larch forest is estimated to be approximately 200 years (Kharuk *et al* 2013).

To calibrate and validate the model, we conducted a 100 year simulation by repeatedly inputting climate

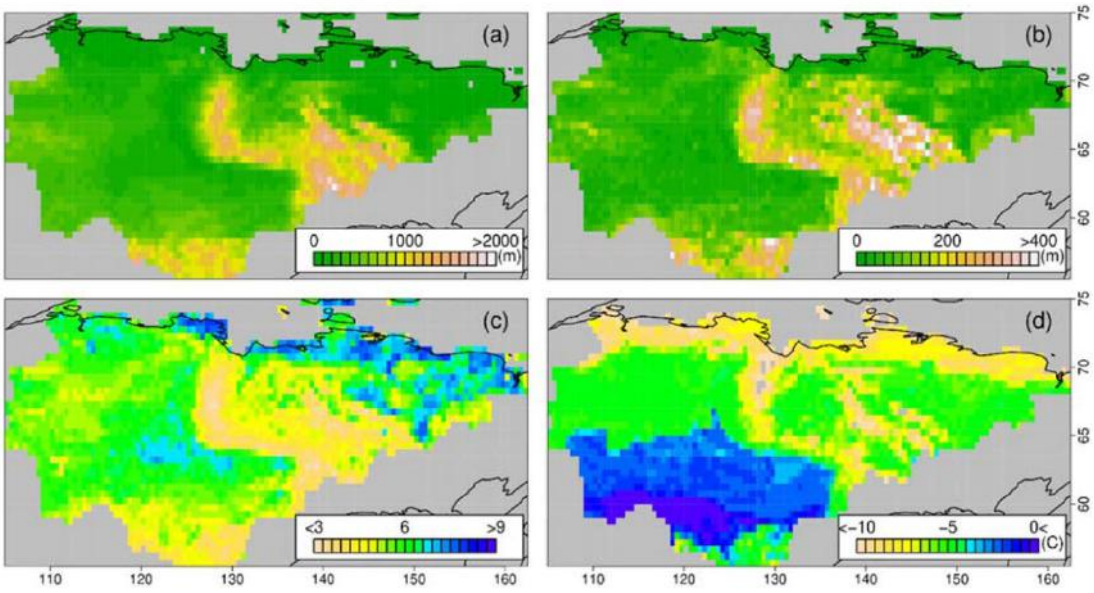

Figure 1. Geographical distribution of environmental data, except climate data, for forcing the simulation. All items are averaged over the 0.5-degree grid and only values of simulation grids are shown. (a) Elevation, (b) Standard deviation of elevation, (c) Combined Topographic Index, and (d) Permafrost temperature. Vertical axes show the latitude and horizontal axes show the longitude. Data sources are shown in tables S1.

data from the last 10 years of the 20th century (1991–2000). Atmospheric CO_2 concentration is assumed to be 368 ppm, which was the observed global average in the year 2000. Each 100 year simulation started from bare ground and assumed no wildfires during this period. The results of the last 10 years of the simulation were averaged and used for validation and calibration.

For calibration, we reconstructed simulation-grid-averages of fundamental properties of plant productivity and thermo-hydrology: annual GPP, canopy LAI in July, ALT, and runoff fractions. Biomass was not used for the calibration, because its estimates in Siberia varies quite much among analysis (Houghton *et al* 2007). The calibration parameters and their assigned values are presented in table S3. The comparison of observation-based-estimates and simulated values (averages of simulation grids) is available in table S4. To validate the calibrated model, we compared geographical distributions of calibrated variables and living biomass between observation-based-estimates and simulated values. The geographical distribution of runoff fraction was not employed here, as it shows artificially binominal distributions (figure 2(i)). The calibrated model roughly reproduced the geographical distributions of the calibrated variables and biomass (figures 2 and S2), which demonstrated that the model reasonably responds to environmental gradients in eastern Siberia. Correlation coefficients (CCs) between observation-based-estimate and simulated values were 0.622 for tree LAI in July, 0.802 for annual GPP, 0.635 for biomass, and 0.584 for ALT.

2.5. Simulation and analysis

With the calibrated model, three different simulations were conducted under both current and future climatic conditions: (1) control run, (2) simulation without redistribution of soil water among elevation ranks (hereafter, no redistribution run), and (3) simulation without air temperature adjustment among elevation classes (hereafter, no temperature adjustment run). Except above modifications, all runs were conducted in accordance with the calibration and validation procedures. The 100 year run is not enough for bringing soil carbon pools to a quasi-equilibrium state, however, soil carbon pools do not feedback to the vegetation dynamics and thermo-hydrology in this model.

The comparisons of the three simulations are referred to as 'model experiment' in this study. To demonstrate how model modifications enable the reconstruction of within-grid heterogeneity, we calculated the CCs between the elevation rank and larch LAI and between the elevation rank and ALT for each half degree grid cell.

We also conducted a sensitivity test for the assumption of fire return interval on the simulation results: 50 and 200 year old forests were simulated and compared with a forest stand 100 years from bare ground (control run). Except for the simulation period, both runs were conducted in accordance with the control run.

Finally, we conducted a simulation using a forecasted climatic condition of the 21st century with MIRIC-GCM (Watanabe *et al* 2011) under the RCP 8.5 IPCC scenario. The 100 year simulations started

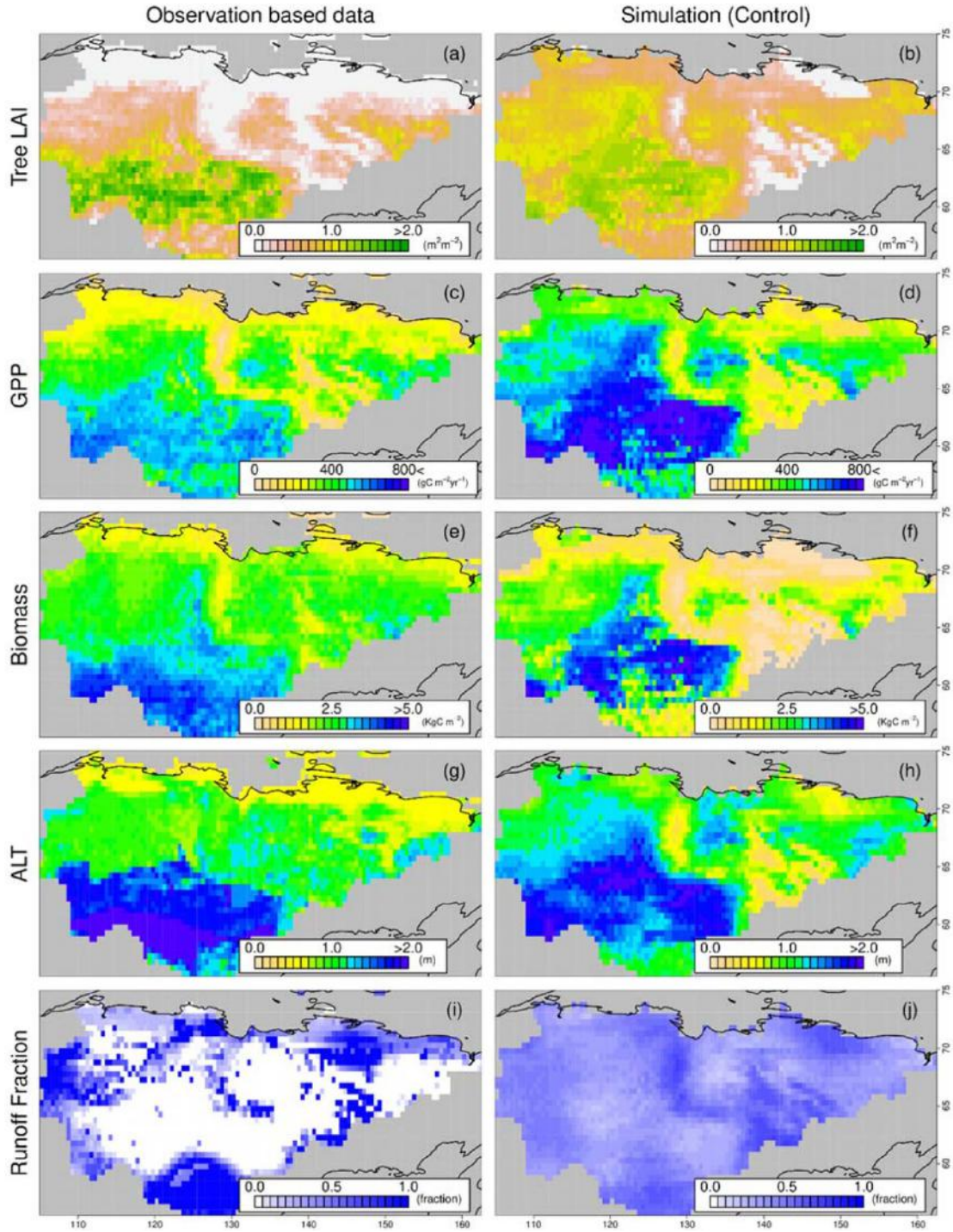

Figure 2. Comparisons of observation-based data and simulation outputs for the validation of the simulation. All items are averaged over the 0.5-degree grid and only values of simulation grids are shown. (a), (b) Larch LAI in July, (c), (d) annual Gross Primary Production (GPP), (e), (f) biomass, (g), (h) Active Layer Thickness (ALT), and (i), (j) runoff fraction. Sources of observation data are shown in tables S2. Simulation was forced with climate data during the last 10 years of the 20th century. Vertical axes show the latitude and horizontal axes show the longitude.

in the year 2001 and the results in the last 10 years (2091–2100) are averaged for evaluation. During the simulation, atmospheric CO_2 concentration changes along with the RCP 8.5 scenario. In accordance with the simulations under historical climate condition, no redistribution run and no temperature adjustment run were conducted under the future climate condition.

3. Results

A clear geographical pattern existed for the CC of elevation rank and tree LAI in the observation-based data. A strong negative trend was observed for mountain regions, whereas a weak positive trend was observed for plain regions (figure 3(a)). The modified model qualitatively and partially reconstructed

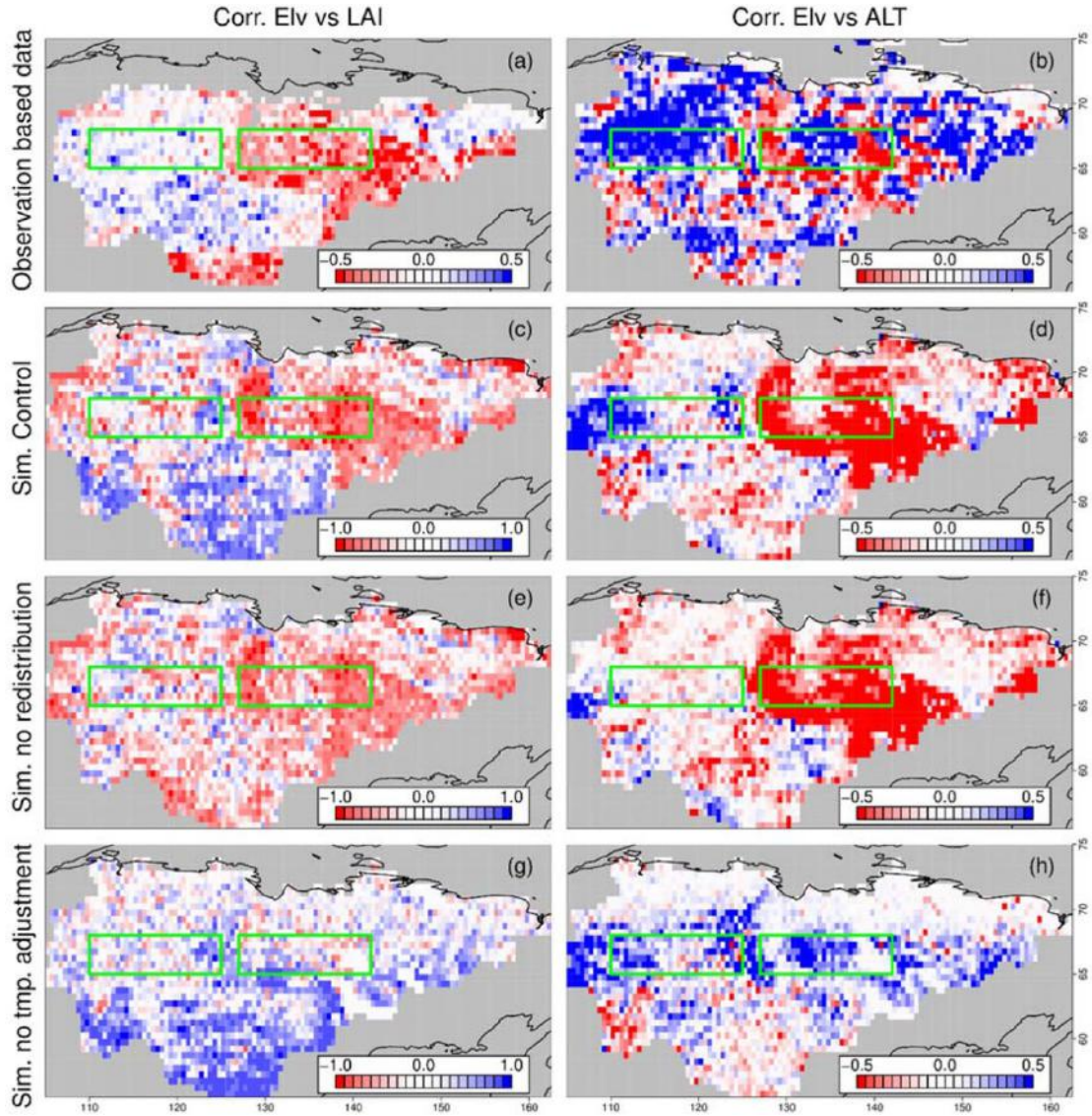

Figure 3. (a), (c), (e), (g) Correlation coefficients between the elevation ranks (Elv) and larch leaf area index (LAI). (b), (d), (f), (h) Correlation coefficients between the Elv and active layer thickness (ALT). (a), (b) Observation-based data. (c), (d) outputs of control simulation. (e), (f) Outputs of simulation without soil water redistribution among elevation ranks. (g), (h) Outputs of simulation without air temperature adjustment among elevation ranks. Rectangular boxes with green line correspond to example plots of plain area (west box) and mountain area (east box), which are used as examples of the effect of elevation ranks on the seasonal patterns of thermo-hydrology and LAI. Vertical axis shows the latitude and horizontal axis the longitude.

this pattern (figure 3(c)), although its magnitude was generally higher than that for the observation-based estimate. The simulated negative CC in mountain regions should be primarily reconstructed by air temperature adjustment among elevation ranks because it nearly disappeared in the no temperature adjustment run (figure 3(g)), whereas it was maintained in the no redistribution run (figure 3(e)). The simulated positive CC in plain regions should be reconstructed by the redistribution of soil water among elevation ranks because the trend nearly disappeared in the no redistribution run (figure 3(e)), whereas it was maintained in the no temperature adjustment run (figure 3(g)).

A geographical pattern also existed for the CC of elevation rank and ALT in the observation-based data. A negative trend was observed for mountain regions, whereas a positive trend was observed for plain regions (figure 3(b)). The modified model qualitatively and partially reconstructed the negative CC in the mountain region, whereas it did not reconstruct a consistent CC for the plain regions (figure 3(d)). The positive trend in the mountain region should be reconstructed by air temperature adjustment among elevation ranks because it disappeared in the no temperature adjustment run (figure 3(h)), whereas it was maintained in the no redistribution run (figure 3(f)). The predominant positive trend in the CC occurred in the no temperature adjustment run (figure 3(h)), which indicated that soil water redistribution was responsible.

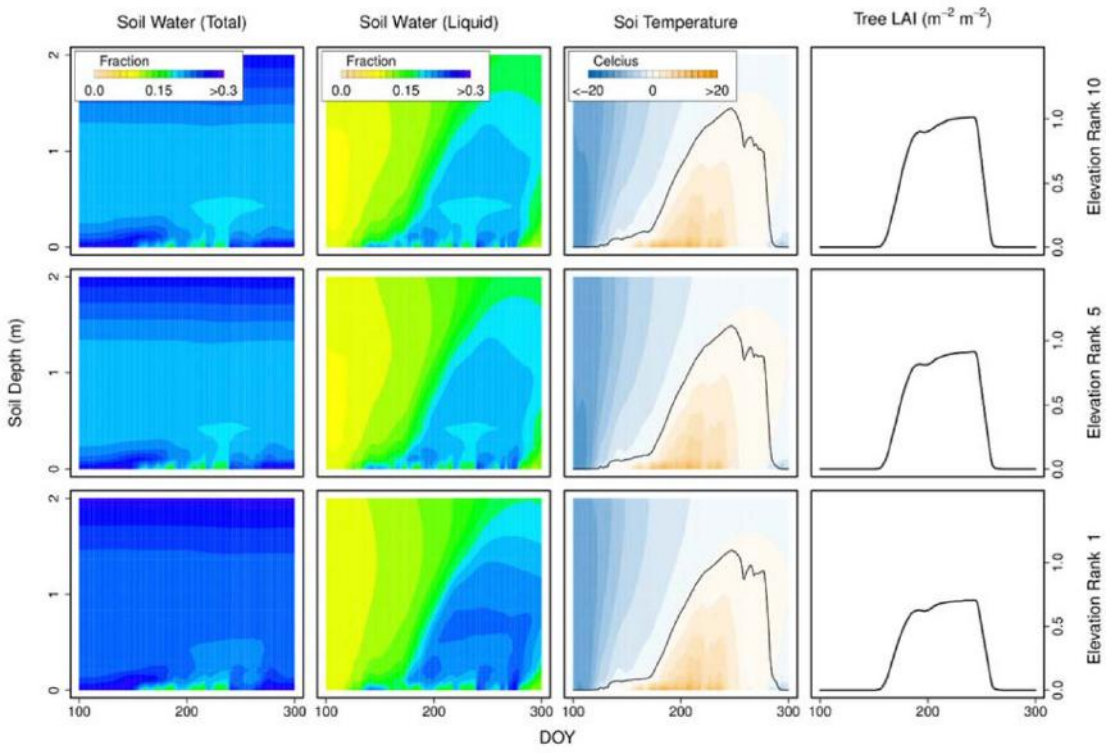

Figure 4. Three rows from left show: seasonal changes in vertical distributions of soil water (ice + liquid states), soil water (only liquid state), and soil temperature, respectively, simulated over example plots of plain area, of which the location is shown in figure 3. This region includes 180 simulation grids, which are averaged for each elevation rank. Rightmost row shows seasonal changes in LAI simulated over the same area. Panels on top, middle, and low columns, show simulation results averaged over elevation rank 10 (highest), 5 (near average), and 1 (lowest), respectively. Solid lines on the soil temperature show active-layer-thickness. Unit of water content 'fraction' indicates fraction of soil volume.

To evaluate how these different patterns occur between mountain and plain regions, seasonal changes in thermo-hydrological status were compared between mountain and plain example areas. The locations are shown in figure 3. Roughly consistent with figure 3(c), tree LAI was higher at higher elevation ranks in the plain area (figure 4), whereas the opposite trend occurred in the mountain area (figure 5). For both the plain and mountain regions, the content of liquid soil water was higher at lower elevation ranks, whereas its maximum value at within tree root depths (0–0.5 m) was higher for the plain region than for the mountain region. The soil layer within thaw depth was near-saturated with soil water at the lowest elevation rank of the plain area. Roughly consistent with figure 3(d), thaw depth was shallower at higher elevation ranks for the mountain region (figure 5), whereas no clear trend occurred with elevation ranks in plain regions (figure 4).

In the grid averages of the simulation result under the historical climate condition, soil water redistribution increased tree LAI, GPP, and biomass, whereas it decreased the runoff fraction (figure S3). The decrease of runoff with increase of plant productivity generally occurs in the simulations of the SEIB-DGVM, because higher LAI intercepts more rain fall, and higher photosynthesis rate consumes more soil water. These changes were only conspicuous in the plain regions. Soil water redistribution also increased ALT, except for in the southern mountain region. However, temperature adjustment did not bring noteworthy change to the grid averages (figure S3).

Comparison of simulated forests of different ages showed that older forests have larger tree LAI, GPP, and biomass, while slightly shallower ALT and slightly smaller fraction of runoff (figures 2 and S4). In the CC between elevation rank and tree LAI, its positive trend in plane regions became weak and eventually became negative in older forest (figure S5), although this change was much less apparent compared to those of LAI, GPP, and Biomass. In the CC between elevation and ALT, no substantial changes occurred with forest age (figure S5).

Under the forecasted climatic condition during 2091–2100, tree LAI becomes denser for the whole simulation areas in the control run (figures 6(a) and (b)). The no temperature adjustment run did not have a noticeable difference from the control run (data not shown). In the no water-redistribution run, an intense decreasing trend occurs for the whole simulation areas, except for high elevation and northern coast regions around longitude E140–160 (figure 6(d)). Under the control run of future climate, the lowest elevation rank of both plain (figure S6) and mountain (figure S7) regions are nearly saturated

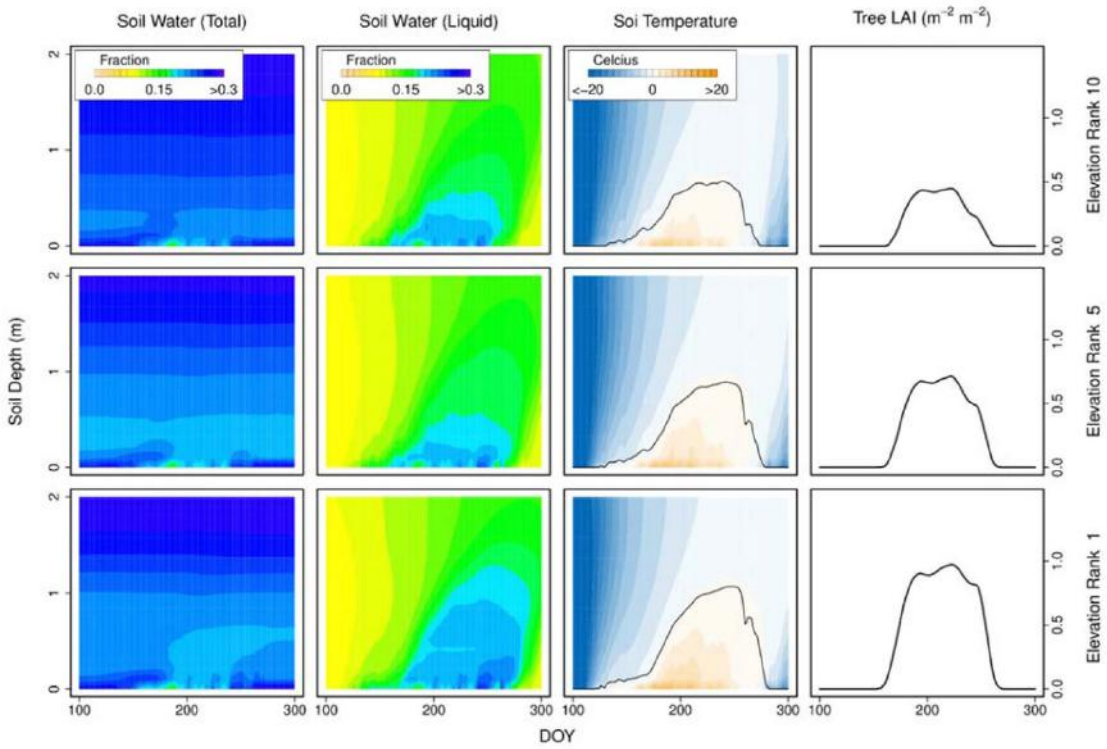

Figure 5. Same as .figure 4, except for simulation results of example plots of mountain areas, of which the location is shown in figure 3

with soil water status in its ALT, which will kill trees. Higher elevation ranks have much lower soil wetness. Under the no-water-redistribution run of future climate, ALT saturation of soil water occurs in both plain (figure S8) and mountain (figure S9) regions irrespective of elevation ranks, which is responsible for their low tree LAI.

4. Discussion

4.1. Reconstruction of tree LAI differences among elevation class

The model reconstructs the topography control on tree abundance; negative correlations between elevation rank and larch LAI in mountain regions (figure 3(a)) were partially reconstructed by the control run (figure 3(c)). The model experiment showed that this reconstruction was a result of air temperature adjustment with elevation, of which the intensity was higher for the mountain region, with its high within-grid deviation of elevation (figure 1(b)), than in the plain region. In the simulations of eastern Siberia, colder environment generally decreased simulated larch LAI through a shorter growing season, lower photosynthesis efficiency, and shallower ALT; and accompanied by lower water holding capacity in the soil (Sato *et al* 2016). However, the model did not reconstruct the positive correlation in the southernmost mountain region around latitude N56–59 in the simulation. This area had an approximately 10 °C higher annual-mean-temperature (figure S1(a)) than the central mountain region and more than 500 mm of annual precipitation (figure S1(c)). This climatic combination would inhibit the above mechanisms for the downregulation of tree LAI.

The model experiment showed that within-grid soil water redistribution was responsible for reproducing positive correlations between elevation and larch LAI in plain areas. This positive correlation should be caused by the combination of soil water redistribution and over-wet-kill of trees, of which the condition was calibrated with tree mortality observed at the Spasskaya Pad experimental forest during August 2006 (SI2). Our simulation demonstrated that the same extent of this moist condition can occur throughout simulated plain areas under the climate condition at the end of the 21st century.

4.2. Reconstruction of ALT differences among elevation classes

The observation-based data showed the trend that ALT becomes shallower in higher elevation areas in mountainous region (figure 3(b)). This pattern is intuitively understandable because ALT becomes shallower in colder environments and the within-grid temperature difference should be much higher in the mountain regions, which has much higher within-grid heterogeneity of elevation, than in the plain regions (figure 1(b)). The simulation roughly reconstructs this trend and the model experiment showed that this reconstruction is caused by air temperature adjustment with elevation.

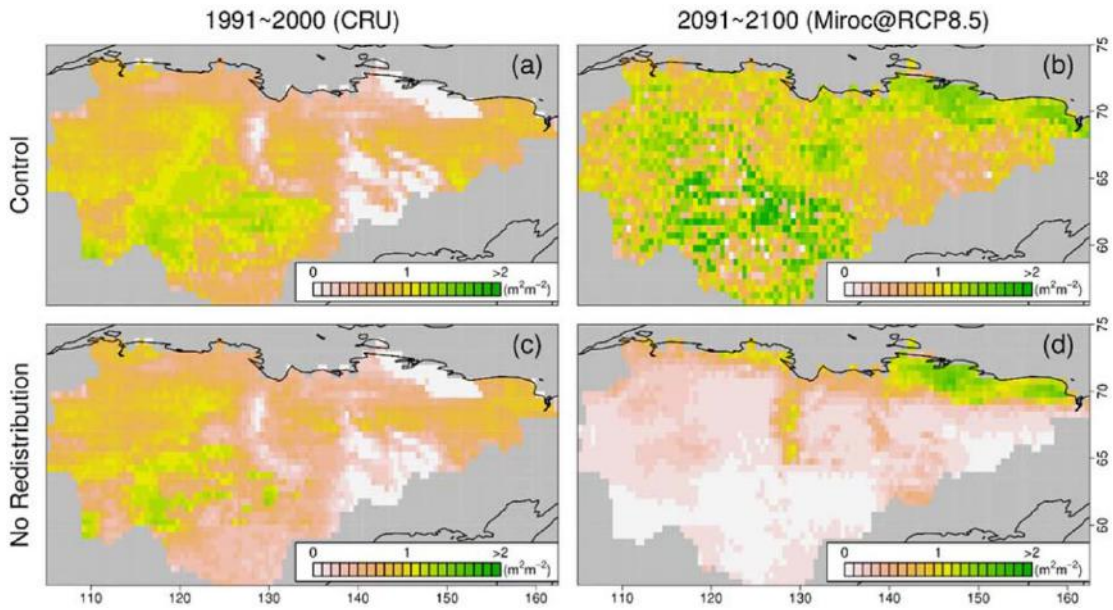

Figure 6. Grid averages of tree LAI under the historical climate during 1991–2000 (a), (c) and the future climate during 2091–2100 (b), (d). Control run results (a), (b) are compared with no-water-redistribution run (c), (d).

The opposite trend was observed in the plain regions; ALT becomes shallower in lower elevation areas (figure 3(b)). Moister environments in lower elevation classes would explain this pattern. Observational studies on arctic Canada have demonstrated that wetland soil has a shallower ALT than drier sites and this pattern is caused by the fact that wetland soil has a larger ice content, which requires more energy to thaw. Additionally, a larger ice content facilitates downward heat conduction to permafrost; heat conductance of ice is approximately four times larger than that of liquid state water (Woo and Xia 1996, Carey and Woo 1998). The model experiment generated a trend consistent with the above explanation; soil water redistribution among elevation classes generally results in shallower ALT in lower elevation areas (figure 3(h)), where ice saturation in soil happens during winter (figure 4). However, the model failed to reconstruct the geographical distribution of the negative correlation (figure 3(b) and (d)).

4.3. Sensitivity test for forest age

We evaluated simulated forests at 100 years old, which can be regarded as half of the average frequency of stand-replacing fire in Siberia (Kharuk *et al* 2013). However, much uncertainty remains in the estimate due to the complicated nature of wild fires in this region. For example, the average of overall fire frequency is 15 years, ranging from 4 to 43 years, and has not been observed to exceed 50 years (Katamura *et al* 2009). However, about 80% (Conard and Ivanova 1997) to 93% (Isaev *et al* 2002) of the area burned is thought to be surface fires, which only consumes litter and surface vegetation. In permafrost areas, wildfires deliver significant impacts on the forest conditions as well as hydrology (Yoshikawa *et al* 2003, Jafarov *et al* 2013). Indeed, forest age gave substantial influences on larch LAI, GPP, and biomass in our simulations (figures 4 and S4). In contrast, forest age provided only small or negligible influences on topographical controls on larch LAI and ALT within grid scale (i.e. CC between elevation rank and larch LAI, and CC between elevation rank and ALT) (figure S5). Although each simulation assumes that all forests had the same age, this high independency would demonstrate that our validation strategy, which employs these CCs, is robust against the assumption for forest age.

4.4. Further effort required for better simulation

The model cannot reconstruct the geographical distribution of the positive correlation between elevation and ALT (figures 3(b) and (d)). Additionally, the simulated CCs between elevation rank and larch LAI were much higher than those of the observation-based data (figures 3(a) and (c)). For a more accurate reconstruction of thermo-hydrology and vegetation distribution, further efforts are required to address issues below.

Part of the reason for this limited accuracy can be attributed to the assumption that elevation class represents all environmental heterogeneity within a grid. Another part of the reason for the inaccurate reconstruction can be attributed to the assumption that all forests had the same age in our simulation. This is because vegetation can alter thermo-hydrology dynamics through processes that involve canopy shading, snow interception, and litter accumulation, which function as effective thermal insulants between the soil and atmosphere (Jorgenson *et al* 2010).

Indeed, observational studies have shown that seasonal maximum of ALT is the highest immediately after stand replacing fire and gradually becomes shallower with the recovery of forest (Sato *et al* 2016). This is consistent with the fact that stand replacing fires in the Siberian larch forest consume most of the surface soil organic layer, of which the depth is typically 10–25 cm in mature forests (Sofronov and Volokitina 2010). Consistently, in permafrost ecosystems in Alaska, canopy removal following fire increases both ground heat flux (Chambers and Chapin 2003, Liu *et al* 2005) and ALT (Viereck 1982).

Interactions between thermo-hydrology and vegetation can occur at finer geographical scales (Walvoord and Kurylyk 2016); hence, it is challenging to simulate its behavior at the geographical scale of eastern Siberia. For example, Hinkel (2003) noted the need for specific small-scale studies to understand the causes of the significant intra-site variation in ALT and to simulate moisture conditions found at the larger scale. Indeed, Wright *et al* (2009) showed that ALT is highly variable over a relatively short distance (0.25–1 m) and spatial variability is strongly correlated to soil moisture distribution, which is partially influenced by lateral flow converging to frost table depressions.

Finally, the projected influences of near-surface-permafrost thaw on the existence of the larch forest differ among studies. For example, permafrost decay results in enhanced plant productivity for Siberian larch forest with a modified LPJ-DGVM (Beer *et al* 2007), because a deeper ALT would increase the water holding capacity. However, in the dynamic vegetation model of Zhang *et al* (2011), permafrost thaw results in the collapse of the Siberian larch forest because of the rapid drainage of soil water, which causes a large water deficit in summer. Therefore, more effort is required to improve thermo-hydrological representations for a better projection of the Siberian larch forest in a changing climate.

4.5. Simulation under a forecasted climate condition

In the control run, water redistribution should reduce the risk of over-wet-kill for larch trees in higher elevation classes, whereas it should increase this risk in lower elevation classes. In our simulations, the former effect should be higher than the latter one because water redistribution among elevation classes slightly increased the grid average of larch LAI in the plain areas under the climate of 1991–2000 (figures 6(a) and (c)) and significantly increased the grid average of larch LAI in nearly all simulated areas in the climate of 2091–2100 (figures 6(b) and (d)). This significant difference between the 20th and 21st centuries demonstrates that the 'refugia' effect in higher elevation patches becomes substantial under the trends of increasing annual mean temperature and precipitation, which are forecasted throughout eastern Siberia during the 21st century (figures S1(b) and (d)).

In our previous study using the original SEIB-DGVM, which ignores both over-wetting-kill and topographic heterogeneity within simulation grids, larch biomass increases under the forecasted climatic trends of the MIROC-based projection under the RCP 8.5 (Watanabe *et al* 2011) as a result of growing season extension and reduced water shortages (Sato *et al* 2016). This simulation also shows an increasing trend of soil water content during the growing season of larch; hence, it may result in the reduction of larch biomass if over-wet-kill is taken into consideration without the consideration of topographic heterogeneity. This study demonstrates the risk of overestimating over-wet-kill without the consideration of topographic heterogeneity within simulation grids.

5. Conclusion

The modified model partially reconstructs the topography control on tree abundance; a negative correlation between elevation and canopy LAI in the mountain region but a positive correlation in the plain regions. Additionally, the modified model partially reconstructs topography control on ALT; a negative correlation between elevation and ALT in the mountain region but a positive correlation in the plain regions. The model experiment shows that the positive correlations in the mountain region are the results of air temperature adjustment with elevation, whereas the negative correlations are the results of the combination of soil water relocation along elevation and over-wet-kill of trees. These mechanisms, which contribute to the reconstruction of observation trends, may be consistent with the actual mechanism in nature. However, the model has poor performance for the qualitative reconstruction of the geographical distribution of topographic controls on canopy LAI and ALT, which indicates the need for further effort to develop a more accurate representation of the interactions between climate and vegetation conditions on the thermo-hydrology dynamics.

We demonstrated, in a forecasted climatic condition of the 21st century, that the future may hold a much moister environment throughout eastern Siberia, which is enough to cause ubiquitous tree death owing to over-wet stress. Modeling the over-wet-kill of trees without the consideration of topography heterogeneity may result in the overestimation of forest collapse caused by over-wet-kill of trees under the expected climate trend in eastern Siberia. Applicability of this method in other permafrost ecosystems would also be worth exploring.

Acknowledgments

This research was financially supported by (1) JSPS KAKENHI [Grant Number 17K00540], (2) Arctic Challenge for Sustainability (ArCS), and (3) Strategic International Research Cooperative Program, Japan Science and Technology Agency (JST). C.B. acknowledges financial support by Deutsche Forschungsgemeinschaft (DFG, German Research Foundation)—BE 6485/1-1. Natural Environment Research Council supplied 1-arc second global topographic index values. We would like to thank anonymous reviewers for for comments on the manuscript.

Data Availability Statement

The data and code that support the findings of this study are openly available at the following URL/DOI: https://doi.org/10.5281/zenodo.3830370.

References

Beer C, Fedorov A N and Torgovkin Y 2013 Permafrost temperature and active-layer thickness of Yakutia with 0.5-degree spatial resolution for model evaluation *Earth Sys. Sci. Data* **5** 305–10

Beer C, Lucht W, Gerten D, Thonicke K and Schmullius C 2007 Effects of soil freezing and thawing on vegetation carbon density in Siberia: A modeling analysis with the lund-potsdam-jena dynamic global vegetation model (LPJ-DGVM) *Global Biogeochem. Cycles* **21** 1

Beven K J and Kirkby M J 1979 A physically based, variable contributing area model of basin hydrology/Un modèle à base physique de zone d'appel variable de l'hydrologie du bassin versant *Hydrol. Sci. Bull.* **24** 43–69

Bonan G B, Chapin F S and Thompson S L 1995 Boreal forest and tundra ecosystems as components of the climate system *Clim. Change* **29** 145–67

Carey S K and Woo M-K 1998 A case study of active layer thaw and its controlling factors *7th Int. Permafrost Conf.* pp 127–32

Chambers S D and Chapin F S 2003 Fire effects on surface-atmosphere energy exchange in Alaskan black spruce ecosystems: implications for feedbacks to regional climate *J. Geophys. Res. Atmos.* **108** D1

Cohen J *et al* 2014 Recent Arctic amplification and extreme mid-latitude weather *Nat. Geosci.* **7** 627–37

Conard S G and Ivanova G A 1997 Wildfire in Russian boreal forests - Potential impacts of fire regime characteristics on emissions and global carbon balance estimates *Environ. Pollut.* **98** 305–13

Ek M B, Mitchell K E, Lin Y, Rogers E, Grunmann P, Koren V, Gayno G and Tarpley J D 2003 Implementation of Noah land surface model advances in the national centers for environmental prediction operational mesoscale Eta model *J. Geophys. Res. Atmos.* **108** D22

Gedney N and Cox P M 2003 The sensitivity of global climate model simulations to the representation of soil moisture heterogeneity *J. Hydrometeorol.* **4** 1265–75

Gibbard S, Caldeira K, Bala G, Phillips T J and Wickett M 2005 Climate effects of global land cover change *Geophys. Res. Lett.* **32**

Harris I C, Jones P D, Osborn T J and Lister D H 2014 Updated high-resolution grids of monthly climatic observations - The CRU TS3.10 dataset *Int. J. Climatol.* **34** 623–42

Harris I C, Osborn T J, Jones P D and Lister D H 2020 Version 4 of the CRU TS monthly high-resolution gridded multivariate climate dataset *Sci. Data* **7** 109

Hinkel K M 2003 Spatial and temporal patterns of active layer thickness at circumpolar active layer monitoring (CALM) sites in northern Alaska, 1995–2000 *J. Geophys. Res.* **108** D2

Houghton R A, Butman D, Bunn A G, Krankina O N, Schlesinger P and Stone T A 2007 Mapping Russian forest biomass with data from satellites and forest inventories *Environ. Res. Lett.* **2** 045032

Isaev A S, Korovin G N, Bartalev S A, Ershov D V, Janetos A, Kasischke E S, Shugart H H, French N H F, Orlick B E and Murphy T L 2002 Using remote sensing to assess Russian forest fire carbon emissions *Clim. Change* **55** 235–49

Jafarov E E, Romanovsky V E, Genet H, Mcguire A D and Marchenko S S 2013 The effects of fire on the thermal stability of permafrost in lowland and upland black spruce forests of interior Alaska in a changing climate *Environ. Res. Lett.* **8** 035030

Jorgenson M T, Romanovsky V, Harden J, Shur Y, O'Donnell J, Schuur E A G, Kanevskiy M and Marchenko S 2010 Resilience and vulnerability of permafrost to climate change *Can. J. For. Res.-Rev. Canadienne De Recherche Forestiere* **40** 1219–36

Kalnay E *et al* 1996 The NCEP/NCAR 40-year reanalysis project *B. Am. Meteorol. Soc.* **77** 437–71

Katamura F, Fukuda M, Bosikov N P and Desyatkin R V 2009 Forest fires and vegetation during the Holocene in central Yakutia, eastern Siberia *J. Forest Res.* **14** 30–36

Kharuk V I, Dvinskaya M L and Ranson K J 2013 Fire return intervals within the northern boundary of the larch forest in Central Siberia *Int. J. Wildland Fire* **22** 207–11

Kleinen T, Brovkin V and Schuldt R J 2012 A dynamic model of wetland extent and peat accumulation: results for the Holocene *Biogeosciences* **9** 235–48

Lawrence D M and Slater A G 2005 A projection of severe near-surface permafrost degradation during the 21st century *Geophys. Res. Lett.* **32** 24

Liu H P, Randerson J T, Lindfors J and Chapin F S 2005 Changes in the surface energy budget after fire in boreal ecosystems of interior Alaska: an annual perspective *J. Geophys. Res. Atmos.* **110** D13

Marthews T R, Dadson S J, Lehner B, Abele S and Gedney N 2015 High-resolution global topographic index values for use in large-scale hydrological modelling *Hydrol. Earth Sys. Sci.* **19** 91–104

Sato H and Kobayashi H 2018 Topography controls the abundance of siberian larch forest *J. Geophys. Res. Biogeosci.* **123** 106–16

Sato H, Kobayashi H, Iwahana G and Ohta T 2016 Endurance of larch forest ecosystems in eastern Siberia under warming trends *Ecol. Evol.* **6** 5690–704

Schulze E D *et al* 1995 Aboveground biomass and nitrogen nutrition in a chronosequence of pristine Dahurian Larix stands in eastern Siberia *Can. J. For. Res.-Rev. Canadienne De Recherche Forestiere* **25** 943–60

Sofronov M A and Volokitina A V 2010 Wildfire Ecology in Continuous Permafrost Zone *Permafrost Ecosystems: Siberian Larch Forests*, ed A Osawa, O A Zyryanova, Y Matsuura, T Kajimoto and R W Wein (Berlin: Springer-Verlag GmbH) pp 59–77

Stieglitz M, Rind D, Famiglietti J and Rosenzweig C 1997 An efficient approach to modeling the topographic control of surface hydrology for regional and global climate modeling *J. Clim.* **10** 118–37

Viereck L A 1982 Effects of fire and firelines on active layer thickness and soil temperatures in interior Alaska *Proc. of the 4th Canadian Permafrost Conf.* (Ottawa: National Research Council of Canada) pp 123–34

Vygodskaya N N *et al* 1997 Leaf conductance and CO_2 assimilation of Larix gmelinii growing in an eastern Siberian boreal forest *Tree Physiol.* **17** 607–15

Walvoord M A and Kurylyk B L 2016 Hydrologic impacts of thawing permafrost—a review *Vadose Zone J.* **15** 6

Watanabe S *et al* 2011 MIROC-ESM 2010: model description and basic results of CMIP5-20c3m experiments *Geosci. Model Dev.* **4** 845–72

Woo M K and Xia Z J 1996 Effects of hydrology on the thermal conditions of the active layer *Nord. Hydrol.* **27** 129–42

Wright N, Hayashi M and Quinton W L 2009 Spatial and temporal variations in active layer thawing and their implication on runoff generation in peat-covered permafrost terrain *Water Resour. Res.* **45** 5

Yoshikawa K, Bolton W R, Romanovsky V E, Fukuda M and Hinzman L D 2003 Impacts of wildfire on the permafrost in the boreal forests of Interior Alaska *J. Geophys. Res. Atmos.* **108** 8148

Zhang N N, Yasunari T and Ohta T 2011 Dynamics of the larch taiga-permafrost coupled system in Siberia under climate change *Environ. Res. Lett.* **6** 2